Effect of plasma-induced surface charging on catalytic processes : application to CO_2 activation

Effect of plasma-induced surface charging on catalytic processes: application to CO_2 activation

To cite this article before publication: Kristof Bal *et al* 2018 *Plasma Sources Sci. Technol.* in press https://doi.org/10.1088/1361-6595/aaa868

Effect of plasma-induced surface charging on catalytic processes: application to CO_2 activation

Kristof M. Bal,[1] Stijn Huygh, Annemie Bogaerts and Erik C. Neyts

Research group PLASMANT, Department of Chemistry, University of Antwerp, Universiteitsplein 1, 2610 Antwerp, Belgium

Understanding the nature and effect of the multitude of plasma-surface interactions in plasma catalysis is a crucial requirement for further process development and improvement. A particularly intriguing and rather unique property of a plasma-catalytic setup is the ability of the plasma to modify the electronic structure, and hence chemical properties, of the catalyst through charging, i.e., the absorption of excess electrons. In this work, we develop a quantum chemical model based on density functional theory (DFT) to study excess negative surface charges in a heterogeneous catalyst exposed to a plasma. This method is specifically applied to investigate plasma-catalytic CO_2 activation on supported M/Al_2O_3 (M = Ti, Ni, Cu) single atom catalysts. We find that (1) the presence of a negative surface charge dramatically improves the reductive power of the catalyst, strongly promoting the splitting of CO_2 to CO and oxygen, and (2) the relative activity of the investigated transition metals is also changed upon charging, suggesting that controlled surface charging is a powerful additional parameter to tune catalyst activity and selectivity. These results strongly point to plasma-induced surface charging of the catalyst as an important factor contributing to the plasma-catalyst synergistic effects frequently reported for plasma catalysis.

[1] Corresponding author, e-mail: kristof.bal@uantwerpen.be

INTRODUCTION

Plasma catalysis, i.e., the combined application of plasma technology and a catalyst, is receiving considerable attention for applications such as greenhouse gas conversion, air pollution control, ammonia synthesis, and hydrocarbon reforming, because of its high flexibility and ability to be operated at much lower temperatures than traditional thermo-catalytic processes.[1] In many cases, a synergistic effect is claimed, i.e., the conversion, yield, energy efficiency or selectivity is observed to be greater than the sum of pure plasma processing of the gas and pure thermal catalysis.[2-5] The mechanisms underpinning this apparent efficiency are not fully understood and must be unraveled to achieve a better understanding of the process and optimize its performance. The key characteristic that sets plasma catalysis apart from either isolated plasma-technological or catalytic approaches is the presence of a strong cross-interaction between the plasma and the catalyst surface, mutually changing each other's properties.

From the perspective of the catalyst, the impact of a plasma can be considered as a perturbation of the catalytic chemistry which, on itself, is already a very complex process with a massive number of chemical and physical degrees of freedom. To untangle all these influencing factors, a "bottom-up" approach based on theoretical atomistic calculations is ideally suited to study the role of the chemical building blocks that make up the overall catalytic process.[6] For traditional catalytic approaches to CO_2 activation, for example, this kind of incrementally improved understanding of increasingly complex technologies has already been extensively demonstrated in the literature, mostly based on density functional theory (DFT) calculations. The first step consists of extensively characterizing the energetic and kinetic parameters of a variety of simple catalyst models, such as flat transition metal surfaces[7-14] and oxide single crystals,[15-23] so that general trends with respect to the chemical properties of these materials can be extracted. Then, a next step concerns the study of

supported metal catalysts, introducing the effect of the catalyst/support interaction as an extension of the work on "pure" materials.[24-27] With this increasing model complexity, however, computational work becomes scarcer, and just a few material combinations have been already studied. Yet, these studies have led to the conclusion that the catalyst/support interface plays a significant role in the catalytic activity of the metal, and that reaction mechanisms on a supported cluster can be quite different from those on a pure metal catalyst.[28] The as such obtained insight from incrementally more complex models highlights the power of computational approaches to increase our understanding of catalytic processes.

In principle, plasma catalysis can be treated as another layer of complexity that is added to the computational model of the catalyst, so as to disentangle the effect of the various mechanisms through which the plasma can interact with the catalytic process. This way, the effect of phenomena such as plasma-generated radicals, excited molecules, ions, photons, electrons and electric fields can be studied in isolation to assess their individual impact and relative importance.[29] So far, this type of work has been mostly limited to the impact of a radical flux from the plasma to the catalyst. Using DFT calculations[30] and molecular dynamics (MD) simulations,[31] it was confirmed that gas phase plasma activation of inert gasses such as CH_4 leads to improved chemisorption,[31] whereas a high surface coverage of plasma-generated radicals can significantly modify the activity of the catalyst towards CO_2 activation.[32,33]

Of the many other possible plasma-surface interactions, perhaps the most intriguing is the ability of a plasma to modify the electronic structure of the catalyst through charging. All surfaces exposed to a gas discharge accumulate a negative charge due to the influx of plasma-supplied electrons, which is much larger than the influx of ions. Although physical models[34] and experiments[35-38] suggest that these surface charges can be quite substantial and long-lived, little to nothing is known about their effect on the chemical properties of the catalysts. Nevertheless, this effect can be expected to be important because catalytic bond breaking and

formation processes are governed by the flow of electrons to and from the surface. Because charging is a fully reversible process that does not modify the catalyst's physical structure, a recent set of plasma-catalytic experiments is particularly intriguing: the synergistic effect is found to also be fully reversible, i.e., no permanent plasma-induced chemical or physical modification of the catalyst is observed, which suggests that surface charging could indeed play a role in this process.[39] Since no direct experimental work in this direction has been carried out, and a controlled set-up to isolate the surface charge effect is difficult to achieve, computational approaches must be applied to gauge its impact on the plasma-catalytic process. Computational approaches to charged catalysts in general are, however, rather challenging, and have only been carried out in the context of electrocatalysts in contact with an aqueous phase,[40,41] or in cases in which the charge is approximated through doping.[42,43]

In this work, the effect of surface charging in plasma catalysis is explicitly investigated for the first time. A new practical methodology to account for a charged periodic surface in DFT calculations is presented and applied to CO_2 activation on a negatively charged supported metal catalyst. As model system, atomically dispersed Ti, Ni and Cu-based transition metal catalysts on a γ-Al_2O_3 (110) surface are considered in order to (1) characterize the structure of single atom catalysts on Al_2O_3 and (2) investigate the CO_2 reduction ability of these catalysts and the dependence of their chemical properties on the nature of the metal. Besides being a very promising class of materials,[44,45] single atom catalysts also allow us to "purify" the model from the structural complexity of larger supported clusters, models of which have many more degrees of freedom and therefore require somewhat arbitrary choices of cluster size, structure and orientation.[24-27] For this reason, using a model based on single metal atoms allows for a fairer and clearer comparison of different catalytic transition metals, although preliminary tests indicate that our general conclusions are unaffected by cluster size. Our results show that the presence of excess electrons in oxide-supported transition metal catalysts

dramatically enhances their reductive ability, exemplified by strongly shifting the thermodynamic balance towards CO_2 dissociation. These results suggest that controlled charging of the catalyst surface could greatly enhance the efficiency of the CO_2 reduction process.

METHODS

General methodology for neutral surfaces

All DFT calculations were carried out with the Quickstep module in the CP2K 4.1 package.[46,47] Energies and forces were computed using the Gaussian and plane wave (GPW) method[48] employing Goedecker-Teter-Hutter (GTH) pseudopotentials[49,50] for the core-valence interactions and a polarized double-ζ (m-DZVP) basis set[51] to expand the Kohn-Sham valence orbitals. An auxiliary plane wave basis set defined by a cutoff of 1200 Ry was used to expand the electron density. Exchange and correlation were treated with the PBE functional,[52] supplemented by Grimme's D3 dispersion correction[53] in its Becke-Johnson damping form.[54] *k* point sampling was limited to the Γ point only. Atomic partial charges were calculated by the self-consistent Hirshfeld-I scheme.[55] Molecular adsorption energies were calculated as $E_{ads} = E_{mol+surface} - E_{mol} - E_{surface}$ and are reported without thermal or zero-point energy corrections. Reaction barriers were estimated with the nudged elastic band method;[56] transition state structures were only optimized for the neutral slabs, and single point calculations were carried out in the case of charged surfaces.

Calculations were carried out on a slab of the γ-Al_2O_3 structure proposed by Digne *et al.*[57] The (110) surface was modeled as a 2 × 2 supercell containing 240 atoms, corresponding to six layers of which the bottom two were kept fixed at their bulk positions. The simulation cell dimensions were 16.1606 × 16.8106 × 40 $Å^3$. Periodic boundary conditions were not applied along the *Z* direction to avoid self-interaction of the slab; calculations involving isolated

atoms or molecules were also carried out in these cell sizes. To achieve the desired partial periodicity of the cell, electrostatics were handled by the Martyna-Tuckerman Poisson solver,[58] which requires the non-periodic cell edge to be at least twice as long as the charge distribution. The surface exposes both coordinatively unsaturated Al and O atoms. Tri- (Al_{III}) or tetracoordinate Al (Al_{IV}) atoms provide Lewis-acidic sites, whereas di- (O_2) and tricoordinate (O_3) surface atoms are Lewis basic. Although the (110) surface termination is the most common, it is not stable in its "dry" form, which is why a hydrated variant was also considered in this work (structure s1a from ref. 59) containing 4 adsorbed water molecules, corresponding to a density of about 3 OH nm^{-2}. This surface is the most stable adsorption configuration of a single adsorbed water molecule per unit cell, which is dissociated into an OH group adsorbed on the Al_{III} site and a proton bonded with an O_2 atom. Comparison of the two surfaces allows assessing the impact of adsorbed water on the properties of the Al_2O_3 support.

Unless noted otherwise, the abovementioned PBE-D3 based methodology was employed for all calculations, but a small subset of structures was re-optimized using different exchange-correlation functionals in order to assess the reproducibility or our results and their dependence on the chosen approximations. These additional calculations employed the D3-corrected revPBE[60] and TPSS[61] functionals, the "plain" uncorrected PBE functional and the PBE-rVV10 functional. This latter functional combines PBE exchange-correlation with the nonlocal van der Waals correlation component of the rVV10 functional,[62,63] and was generated in this work by refitting its *b* parameter[64] against an accurate binding curve of the Ar dimer.[65] A more detailed description of all cross-checks is given the Supporting Information. We find that the sensitivity of our results on the choice of the density functional approximation is very small, and has therefore no impact on the general conclusions presented here.

When MD simulations where carried out, a reduced plane wave cutoff of 400 or 600 Ry and box *Z* length of 25 Å was used, with full periodic boundaries. The equations of motion of the Nosé-Hoover chain were integrated with a 0.5 fs time step. Before production runs, each system was equilibrated for 1 ps at the desired temperature. To overcome the severe time scale restrictions of traditional MD simulations (~10 ps for DFT-based MD) we use the metadynamics-based[67] *collective variable-driven hyperdynamics* (CVHD) enhanced sampling method.[68,69] CVHD biasing forces were calculated and applied with the PLUMED plugin.[66] Bond distortions were biased up to a maximal value of 0.5 (50 % bond elongation compared to equilibrium) through addition of a repulsive Gaussian of height 0.01 eV and width 0.05 every 10 fs, with a well-tempered bias factor of 20. More details about the choice of CVHD parameters can be found elsewhere.[68,69] The boost factors that were obtained range from ~100 at 800 K, to over 3×10^6 at 400 K.

Treatment of charged surfaces

A naive approach to model a charged catalyst surface would be directly mimicking reality, i.e., adding an additional electron to a surface slab model to generate a negative surface charge. Such a straightforward model system, however, is an ill-defined problem because the electrostatic energy of a periodically repeated charged system diverges. Traditional Ewald summation methods avoid this divergence catastrophe by mathematically treating the charged system as if it is immersed in a neutralizing background jellium. Although this a reasonable way to treat homogeneous systems (such as a solvated ion) in which the background charge essentially approximates the effect of a uniform distribution of counterions, it breaks down for systems with an inhomogeneous countercharge distribution.[70] In particular, such a charge distribution will be a poor approximation of a surface exposed to a plasma, in which there is a clear charge separation between de negatively charged surface and the plasma sheat that contains positively charged ions.

This approach also leads to a more accurate description of the electric fields arising from plasma-charged surfaces, modeled as semiperiodic slabs. Besides the previously established impact on the chemistry, a uniform background charge also eliminates any electric field effects, by virtue of it being dispersed homogeneously across the cell.[70] In contrast, an explicit counterion added to the gas phase at a sufficient distance above the surface, with periodic boundaries parallel to the surface, will essentially act as a charged plate of opposite charge and generate an electric double layer. This way, an electric field perpendicular to the surface of a magnitude appropriate to the surface charge density will be naturally obtained as a byproduct of the procedure.

Particularly when charged or highly polarized surfaces are modelled, significant artefacts can arise from improper treatment of periodicity. That is, many studies of surface chemistry employ fully periodic cells, and separate repeated images of the same slab with a vacuum layer to eliminate spurious interactions. While neutral, nonpolar surfaces can be conveniently handled with such a methodology, large inter-slab interactions remain for highly charged or polarized surfaces, even with very large vacuum separations, causing errors even in the order of electronvolts in some cases.[71] Inconsistent adsorption energies in fully periodic cells are also observed for the systems studied in this paper, as shown in the Supporting Information. As mentioned in the previous section, all of our calculations consistently apply periodic boundaries only parallel along the surface, and not along the *Z* direction.

In summary, our approach yields a realistic model of a charged catalyst surface exposed to a plasma because (1) the charge distributions match those of the true system, i.e., a negatively charged surface exposed to a gas phase carrying positive countercharges and (2) an electric field, perpendicular to the surface follows self-consistently from these charge distributions.

The practical realization of this approach in a standard DFT code (CP2K) is as follows. The negative surface charges in this work require a positive countercharge which, in the simplest case, can be a proton. It is, however, not always straightforwardly possible to introduce gas phase ions of specified charge into the simulation box. Indeed, if this approach were attempted in a plane wave DFT code, charge transfer could occur to the point charge due to use of a non-localized basis set, making it impossible to control the charge of the slab; after all, the ground state solution of such a surface+free atom system, given full variational freedom of the electron density, is perhaps not the required charge-separated state. This can be compensated by using a DFT code that expands the Kohn-Sham orbitals in an *atom-centered* (localized) basis: if no basis functions are added on the counterion, no electronic density can spill over, its charge can be precisely controlled and the desired surface charge can be enforced. The method is in principle readily usable in any DFT code that uses localized basis sets (such as the here used CP2K) but has, to the best of our knowledge, not yet been described in the literature.

In the setup adopted in this work, a single additional electron is considered and the countercharge (a proton) is placed at a Z position of 40 Å in a box of dimensions $16.1606 \times 16.8106 \times 100$ Å^3; as discussed in the Appendix, these parameter choices give rise to converged adsorption energies on the charged surface. For the surface model used, a single excess electron corresponds to an electron density of 3.68×10^{17} m^{-2} or a surface charge density of about -0.06 C m^{-2}. Recent measurements[37] on alumina exposed to a multi-filament atmospheric pressure dielectric barrier discharge (DBD) put the plasma-induced surface electron density in the order of 10^{15}–10^{17} m^{-2}, close to values used here. In view of these results, and assuming that the charge penetration depth is no more than 1 nm,[37] the relatively small surface model employed in this work is in fact a realistic approximation of a charged plasma-exposed alumina surface.

RESULTS AND DISCUSSION

Transition metal atom adsorption on the Al_2O_3 support

The Al_2O_3 surface is known to provide strong anchoring sites for adsorbed metal atoms, and is therefore an excellent support material to create stable single atom catalysts.[72-74] For the Ti, Ni, and Cu atoms, different adsorption sites were probed on both the dry and hydrated surface. As discussed in the Supporting Information, additional coordination by adsorbed water has an impact on the adsorption characteristics and relative energetics of the surface sites. However, for all metal/surface combinations, the adsorption configuration in which the metal atom is coordinated by two O_2 atoms (Figure 1a) was found to be the most favorable, and is the only one considered in the following (all configurations and their energies are given in the Supporting Information). The effect of surface hydration (and additional OH coordination, Figure 1b) on the metal adsorption energy is limited (< 10 %), indicating that transition metal bonding at the surface does not depend strongly on the precise hydration degree or pattern. In all configurations and on all surfaces, Ti adsorbs much more strongly on the oxide surface than Ni or Cu, as depicted in Figure 1c.

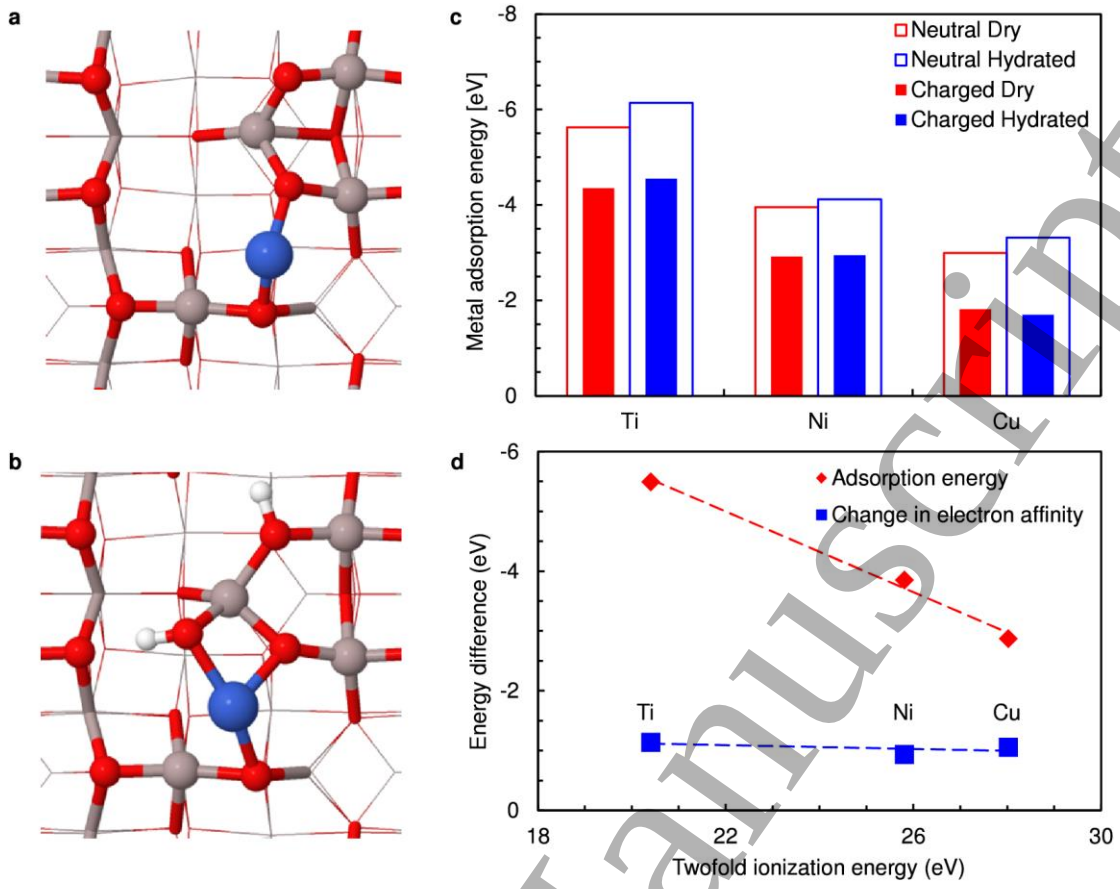

Figure 1: Transition metal adsorption on neutral and negatively charged alumina surfaces. (a) and (b) top view of the most favorable transition metal adsorption configuration on the dry and hydrated surfaces, respectively. Hydrogen: white, oxygen: red, aluminium: gray, and metal: blue. (c) Metal adsorption energies on the two surfaces, with and without extra charge. (d) Correlation of metal binding energies and the change of surface electron affinity $\Delta\chi = E_{ads}(\text{M, neutral}) - E_{ads}(\text{M, charged})$ induced by metal binding with metal ionization energies.

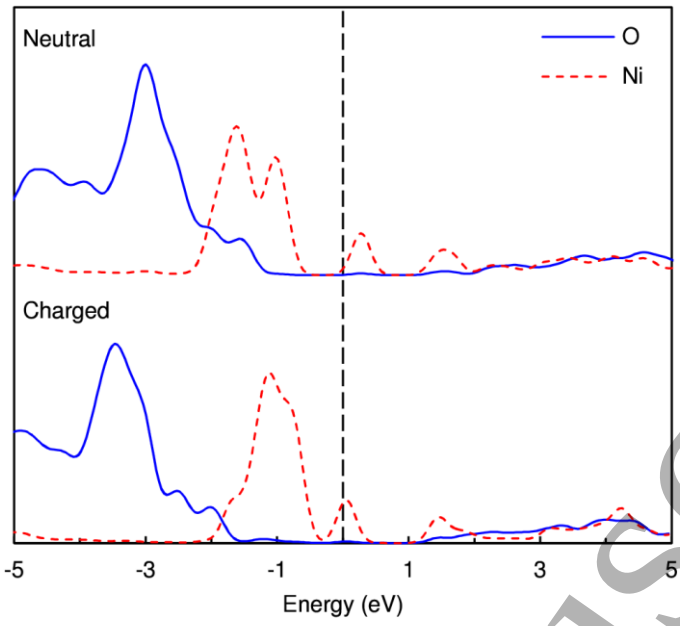

Figure 2: Projected densities of states (PDOS) for Ni supported on the dry surface. Shown are the states of Ni and surface oxygens. Energies are centered on the Fermi level. It can be seen that mixing of metal and surface states is essentially nonexistent.

Transition metal adsorption on the negatively charged surface is not as favorable. The structures of all metal/support combinations were reoptimized with an additional electron, and absolute metal adsorption energies are about 1 eV smaller in all cases or, alternatively, the electron affinity of the support consistently decreases by this quantity when a transition metal atom is adsorbed. In support of the latter phrasing we find two major indications that the metal/support interaction is mostly ionic in character, with the metal atom adsorbed in its M^{2+} state. First, only very limited mixing of the metal and support electronic states is observed in the projected density of states (PDOS, see Figure 2 showing Ni as example), which can be associated with a primarily ionic bond. Second, the adsorption energies of the metal atoms on the dry support correlate very well with their combined first and second ionization energies, i.e., the energetic cost of $M \rightarrow M^{2+} + 2e^-$ in the gas phase (Figure 1d). Combined with the near-constant ~1 eV metal-induced downward shift of the support's electron affinity, it can be inferred that metal atom adsorption on Al_2O_3 is a redox reaction wherein the support is reduced, which therefore becomes more resistant to further reduction through the absorption

of (plasma-supplied) electrons. This reduction of the support upon metal adsorption is of the same magnitude independent of the metal, which is always oxidized to M^{2+} (in this particular configuration), meaning that the support's electron affinity is also modified in the same constant fashion.

CO_2 adsorption

CO_2 can either chemisorb on the metal atom, or on the Al_2O_3 support. In all cases, the adsorbed CO_2 molecule adopts a bent carbonate-like structure, with the O–C–O angle deformed by over 40°, as shown in Figure 3a-b.

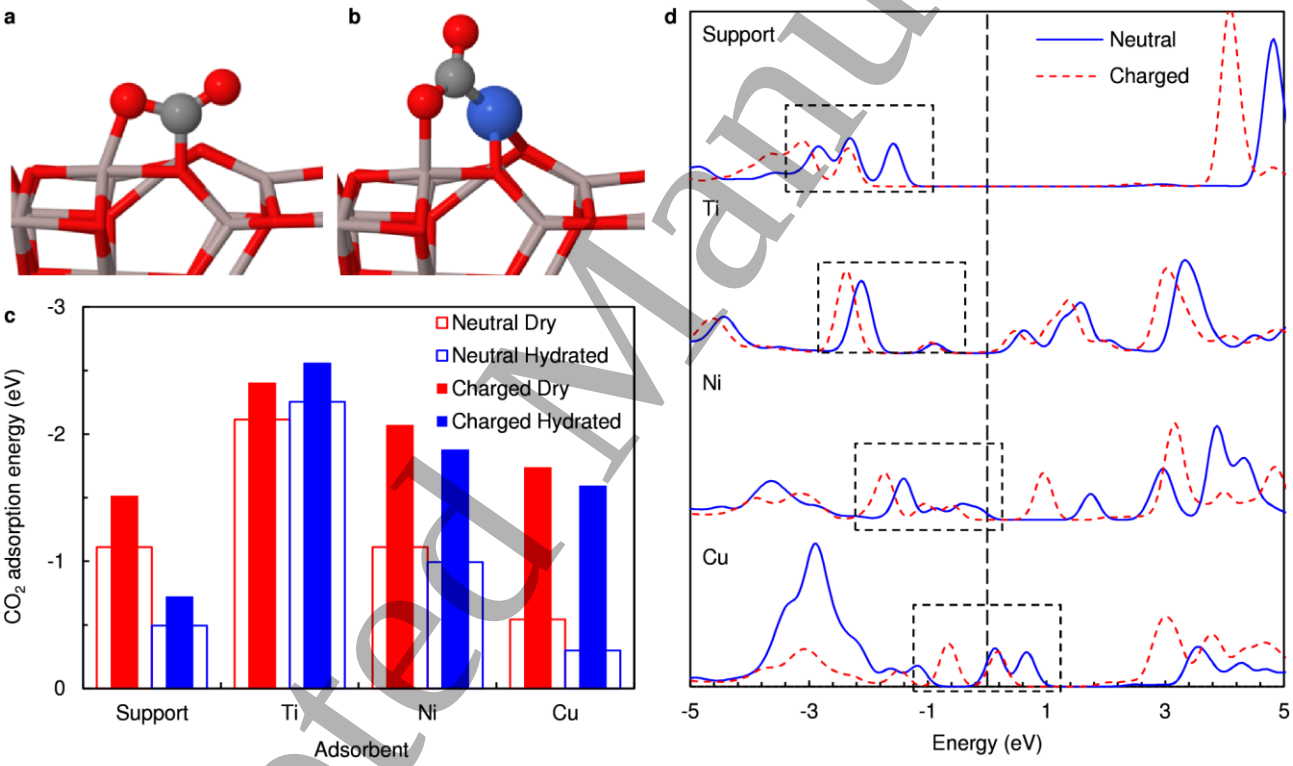

Figure 3: Effect of surface charging on CO_2 adsorption. (a) and (b) Most favorable adsorption configuration on the support and supported transition metal atom. (c) Adsorption energies on all sites, with and without extra charge. (d) PDOS of C in CO_2 adsorbed on all relevant sites on the dry support, centered on the Fermi level (or, rather, the energy of the highest occupied orbital). The relevant high-lying bonding orbitals are marked with dashed boxes.

On the support, the preferential adsorption site is on an Al_{IV}-O_2 Lewis pair, forming Al–O and O–C bonds (Figure 3a). Another configuration involving an Al_{III}-O_2-Al_{IV} site is 0.46 eV less favorable due to the higher Lewis acidity of the Al_{III} site. Indeed, CO_2 is a Lewis acid and

consequently its affinity with a surface site is proportional with the site's basicity, which is why it is typically used as probe molecule to determine surface basicity. In line with this reasoning, the Lewis acidity of the most favorable Al_{IV} site increases upon hydroxylation of Al_{III},[59] correlating with the lower (by 0.62 eV) CO_2 adsorption energy on the hydrated surface. A negative charge transfer, respectively $-0.33e$ and $-0.31e$ on the dry and the hydrated surface, further confirms the Lewis acidic behavior of the CO_2 molecule. CO_2 chemisorption on the γ-Al_2O_3 (110) surface is generally quite similar to adsorption on many other oxides, with adsorption energies in the range of −0.5 to −2.5 eV, formation of a surface carbonate with Lewis basic surface oxygens, strongly bent bi- or tridentate adsorption configurations, and negative charge transfer to the molecule.[15-23] The fairly strong adsorption of CO_2 on the alumina support might also increase the retention time of the molecule near the surface, giving it more time to reach an active catalyst site, although it could also increase the competition between metal and support sites.

For all metal/surface combinations, the IVa adsorption configuration is the most stable, and is therefore used in the CO_2 adsorption calculations. In all cases, CO_2 is found to adsorb in a bridged structure on both the metal atom and the neighboring Al_{IV} surface atom, highlighting the important effect of the support material on the chemical properties of the adsorbed transition metal (Figure 3b). Similar binding modes were observed for larger supported metal clusters, for which the metal/support interface was also the preferred CO_2 adsorption location.[24,25] Ni and Cu exclusively bind the CO_2 carbon atom, whereas the surface Al atom binds one of its oxygen atoms. Ti, on the other hand, forms an η^2 complex with the molecule, coordinating both atoms of a C−O bond, while the Al surface atom coordinates the other C−O bond. The ability of the metal/support interface to provide Lewis acid/base pairs is an important property of oxide-supported metal catalysts that can significantly impact its

reactivity, with the support material playing in active role beyond merely acting as support for the metal catalyst.

The supported metal atoms show a very diverse CO_2 binding behavior, with Ti having the strongest interaction of −2.12 eV (−2.25 eV on the hydrated surface), Ni half as strong with −1.11 eV (−0.99 eV), and Cu even weaker with only −0.54 eV (−0.30 eV), following trends that were established earlier for fcc (100) metal surfaces.[10] In fact, the van der Waals component contributes to about half of the Cu/CO_2 interaction (amounting to 0.22 eV and 0.18 eV on the dry and hydrated surface, respectively), pointing to only very limited chemical bonding, insomuch that adsorption on the alumina support is favored over adsorption on the Cu atom. On the dry surface, this is also true for Ni, although hydration greatly diminishes the support's CO_2 adsorption ability and favors adsorption on supported Ti or Ni (at least for the particular hydration pattern employed here).

Introduction of an additional electron has a dramatic impact on the adsorption properties, significantly improving the binding characteristics of all CO_2 adsorption modes. The magnitude of the effect is the most striking in the case of Cu, which (on the hydrated surface) sees a four-fold increase of the binding energy upon charging, even becoming competitive to Ni. In general, surface charging appears to somewhat "level out" the differences between the metal catalysts, because the effect is much weaker for Ti, which already shows very strong binding with neutral charge.

From a Lewis acid/base theory perspective, negatively charging the surface will naturally increase its basicity and hence improve the binding with the acidic CO_2 molecule. To explain the differences between the adsorption modes, their electronic structure must however be analyzed. In particular, examination of the bonding states in the PDOS, and their position relative to the Fermi level is useful here. The comparatively minor surface charging effect on

adsorption on the dry support can be attributed by the fact that the highest bonding state, formed by overlap of CO_2 antibonding π^* orbitals with surface *p* or *d* states, is fairly low-lying, centered around −2.55 eV (relative to the Fermi level) and shifting to −3.31 eV upon charging; similar observations can be made for CO_2 adsorption on supported Ti (−2.13 eV dropping to −2.38 eV). In contrast, the bonding M−CO_2 states of the neutral dry Ni and Cu-based catalysts lie partially above the Fermi level, especially explaining the very limited Cu−CO_2 bonding: the lower the energy of the metal *d* states, the more difficult they overlap with the high-lying CO_2 antibonding π^* orbitals, resulting in a higher energy (i.e., less stabilization) of the bonding states. Surface charging can therefore have a much larger impact in these cases, lowering the bonding states from −1.00 to −1.43 eV (Ni), and from 0.46 to −0.28 eV (Cu), relative to the energy of the highest occupied orbital. The relative lowering of the bonding states upon charging is also reflected by the charge of the adsorbed CO_2 molecule: increased occupation of these orbitals, which are partially localized on the molecule, leads to a larger electron density; for example, the charge of CO_2 adsorbed on Cu on the hydrated surface changes by −0.27 upon surface charging, compared to only −0.08 and −0.12 on Ti and Ni, respectively.

Although we have primarily focused on supported single atoms, it is instructive to assess to what extent our extensive conclusions for these systems might be valid for larger supported clusters. In a general sense, introducing larger clusters defeats the purpose of using single atoms: the number of degrees of freedom increases with the number of metal atoms in the cluster, meaning that results could become more and more influenced by the choice of the configurations used in the calculations, in contrast to the rather limited set of structures that must be considered in the case of single atom catalysts. Therefore, these initial calculations cannot offer the same fine-grained level of conclusions that has been reached for supported

single atoms but, rather, reveal if our previous conclusions are not an artifact of the particular (pragmatic) choice of catalyst model.

Table 1: Charge effect on CO_2 by a supported Cu_{13} cluster. Energies (eV) of a Cu_{13} cluster adsorption (in a particular configuration) on the dry Al_2O_3 surface, and of CO_2 adsorption and activation on this cluster.

	Neutral	Charged
Cu_{13} adsorption on Al_2O_3	−6.13	−5.63
CO_2 adsorption on Cu_{13}	−0.78	−1.16
CO_2 split on Cu_{13}	−0.12	−0.15
CO desorption from Cu_{13}	1.70	1.87
Overall CO_2 splitting	0.79	0.56

We investigated the charging effect on the properties of a supported icosahedral Cu_{13} cluster, bound on the surface by three O_2 surface atoms and one O_3 site. Upon absorption of an electron most of the additional charge is localized in the cluster, which is changed by $-0.79e$, and a destabilization of 0.5 eV is observed (Table 1). As the studied CO_2 binding mode we considered a bridged structure at the metal/support interface, in analogy with the structures obtained on the single atom catalysts (Figure 4). Again, as evidenced by Table 1, the trends observed for the single atom catalysts are retained, although in somewhat diminished form. Yet, the overall splitting reaction CO_2 (g) → CO (g) + O (ads) is 0.23 eV more favorable on the negatively charged surface, which is significant.

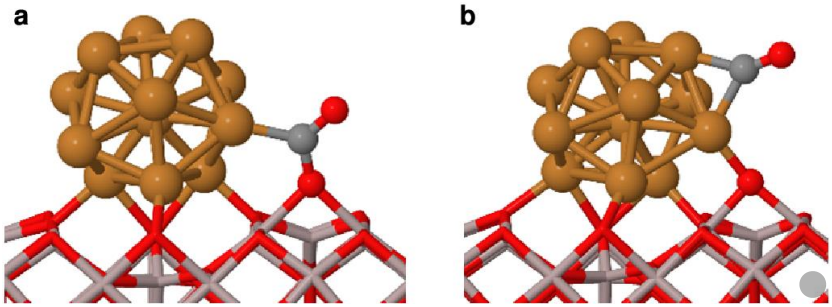

Figure 4: CO_2 splitting on a supported Cu_{13} cluster. (a) CO_2 adsorption configuration, (b) configuration after splitting. The cluster is adsorbed on the dry Al_2O_3 surface.

Adsorption of other molecules on the support

While the Lewis acidic CO_2 shows improved adsorption behavior on a negatively charged substrate, this is not necessarily a good indicator for molecular adsorption in a general sense. Therefore, we calculated the adsorption energies of water, methane, and carbon monoxide on both the neutral and the charged surface, summarized in Table 2. For water, the hydration energy is considered, i.e., the reaction energy of forming the hydrated surface model from the dry surface. Similarly, for methane, dissociative adsorption into CH_3 and H is the studied process. CO is commonly used as basic probe molecule to assess the Lewis acidity of a surface, and is also a major reaction product in CO_2 reduction.

Table 2: Influence of surface charging on molecular adsorption energies (eV) at various sites on the Al_2O_3 support (d: dry surface, h: hydrated surface).

Molecule	Site	Neutral	Charged
H_2O	d-Al_{III}	−2.42	−2.56
CH_4	d-Al_{IV}	−0.38	−0.46
	h-Al_{IV}	0.14	0.11
CO	d-Al_{III}	−1.38	−1.20
	d-Al_{IV}	−1.07	−1.02
	h-Al_{IV}	−1.29	−1.14

Generally, surface charging improves the adsorption behavior of σ-bonded species (H_2O and CH_4), but to a much smaller degree (no more than 0.15 eV) due to absence of unoccupied states close to the Fermi level. CO shows the opposite behavior, consistent with its Lewis basic character, also again showing the relative hydration-induced decrease in basicity for this particular configuration. While CO binds on the surface by donating its lone electron pair on C, a negative surface charge can be donated back to CO by partially filling its antibonding π* orbitals, which become more easily accessible because of the higher energy of the surface electronic states. For example, a CO molecule bound at an Al_{III} surface atom has a total charge of 0.06*e* on the neutral, and 0.02*e* on the charged surface. Hence, in all cases unoccupied states close to the Fermi level play a crucial role in determining the charge dependence on adsorption; the precise direction of the effect depends on their (anti)bonding nature. The implications of these contrasting respective bonding/antibonding interactions in adsorbed CO_2 and CO will be further explored in the following section.

Impact on surface reactions

The uncatalyzed gas-phase splitting of CO_2 (i.e., $CO_2 \rightarrow CO + 0.5\ O_2$) is thermodynamically highly unfavorable (ΔH = 2.9 eV). On a suitable catalyst, the reaction CO_2 (g) → CO (g) + O (ads) can be made more favorable, having a beneficial impact on the overall rate of any process that depends on CO_2 splitting, including dry reforming. Although a structurally simple atomically dispersed catalyst can ostensibly only take part in a small number of reaction mechanisms (direct C−O splitting in this case), the chemical activity of the support material significantly increases the number of possible CO_2 activation pathways. While it is not in the scope of this work to obtain a comprehensive picture of the complete catalytic processes of the considered systems, it is useful to have an initial picture of the most common reactions of adsorbed CO_2.

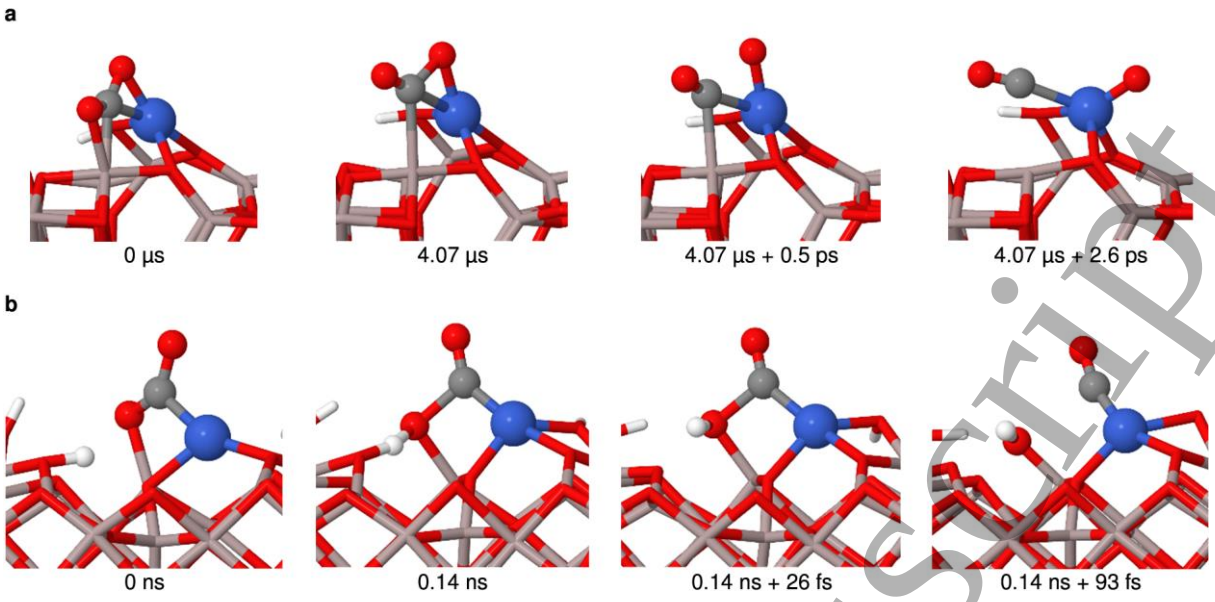

Figure 5: CO_2 splitting by supported metal atoms. Reaction steps observed in CVHD simulations for (a) Ti at 400 K and (b) Ni at 800 K. Accelerated time is given below each frame. Given the time scales, it can be concluded that for Ni, proton transfer and C−O splitting are essentially concerted.

In CVHD-accelerated MD simulations of CO_2 adsorbed on the hydrated Ti-based catalyst, the direct splitting reaction, CO_2 (ads) → CO (ads) + O (ads) (Figure 5a), could be observed at a temperature as low as 400 K (which is indeed typically achieved in a DBD plasma) after a simulated time of 4.1 µs. Ni is not found to be active at 400 K within the CVHD time scale (which does not, however, rule out the general possibility of a reaction), but does react at 800 K after 0.14 ns. However, no *direct splitting* is observed in this case, but rather a *proton-mediated* mechanism in which a proton is first transferred to the CO_2 molecule from an OH group at the support, leading to instantaneous dissociation into CO and OH ((Figure 5b) in a near-concerted fashion.

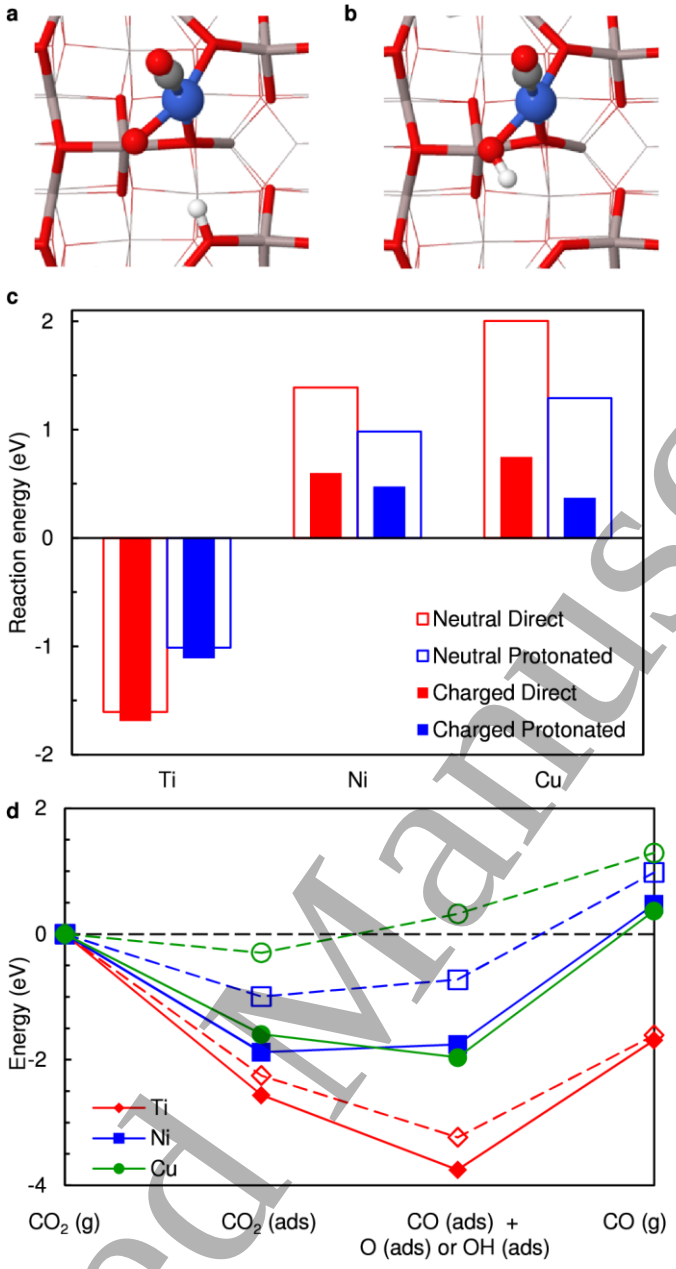

Figure 6: Effect of an excess electron on the reaction energies of CO_2 splitting. (a) Product of the direct splitting reaction. (b) Product of proton-mediated splitting. (c) Overall reaction energies for the two studied mechanisms. (d) Most favorable pathways on all metals. Empty symbols and dashed lines: neutral surface, filled symbols and full lines: charged surface.

Motivated by this apparent difference in the reactivity of Ti and Ni, the overall reaction energies of the two competing CO_2 activation pathways leading to CO (g) + O (ads) and CO (g) + OH (ads), respectively (in their most stable configuration as depicted in Figure 6a and b), were calculated for all metals on both the neutral and charged surface. It is indeed found that Ti is more active towards direct splitting, while Ni and Cu favor a proton-mediated

mechanism (Figure 6c). Also in agreement with the simulations is the much more favorable reaction energy of the initial splitting step on Ti, which reacted at 400 K and exhibits a reaction energy of −0.98 eV, as compared to Ni, which reacted at higher simulated temperatures and has a reaction energy of 0.27 eV. The much higher reactivity of Ti can be attributed to its higher intrinsic reductive abilities: while formally adsorbed in the Ti^{2+} state, a further oxidation to Ti^{4+} is possible, which can be achieved by reducing CO_2.

When examining the effect of an excess electron on the overall splitting process the results largely echo those of CO_2 adsorption, with reactions on Ti relatively unaffected (ΔE_{charge} = −0.08 eV for direct splitting) and the process on Cu exhibiting a very strong influence (ΔE_{charge} = −0.92 eV for proton-induced splitting) by the additional negative surface charge (Figure 6c). Interestingly, when decomposing the energetic contributions of the separate process steps (depicted in Figure 6d), it can be seen that the initial CO_2 adsorption step is in fact the most affected by the charge, while the subsequent steps are not as dissimilar to their counterparts on the neutral surface. Larger effects are observed again for the desorption of CO, which is more strongly bound on the charged than the neutral surface, in contrast to what was found for the adsorption on the support. Indeed, CO_2 always adsorbs through hybridization of its antibonding π^* orbitals with high-lying surface states, giving rise to new bonding states around the Fermi level that can be further stabilized with an excess negative charge. CO, however, interacts with the support through a σ-bonded interaction involving its lone pair, leaving its mostly unmodified π^* orbitals available in an antibonding state that can be occupied by an excess electron, destabilizing the adsorption complex. In contrast, CO interaction with a metal involves a d-π^* overlap that again produces a bonding interaction that will be strengthened by charging. These concepts are illustrated in Figure 7.

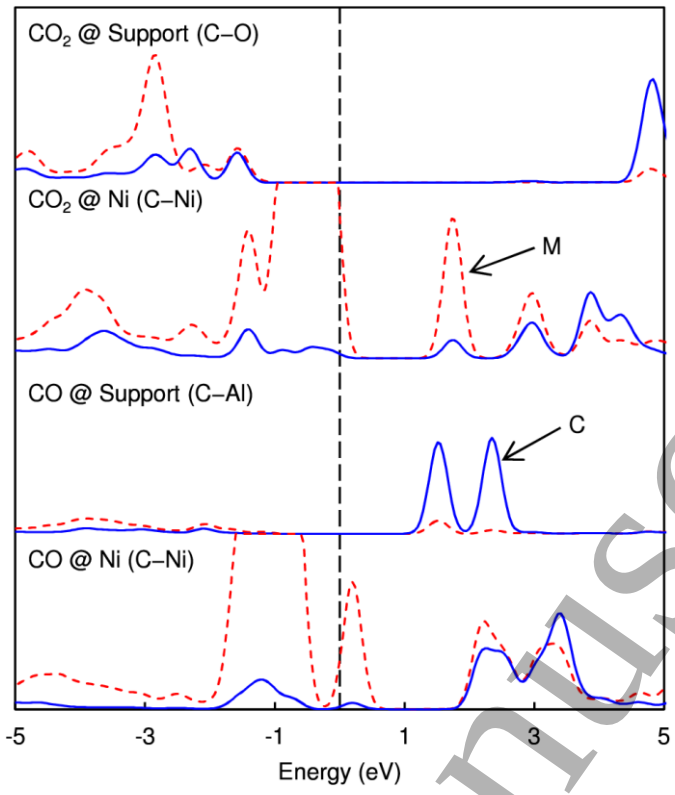

Figure 7: Contrasting adsorption behavior of CO_2 and CO. PDOS of C−M interaction, with M being the surface atom forming a bond with a C atom in the molecule. It can be seen that around the Fermi level, CO_2 π^* states are always hybridized with the surface states, giving rise to new bonding states. This also true for CO bound on a metal atom (here Ni), but not on the support, where the π^* orbitals remain clearly recognizable as such, do not mix appreciably with the surface states, and remain antibonding. Blue lines: C, red dashed lines: M.

While it becomes more difficult to release CO from the metal catalyst upon the charging, the *overall* CO_2 splitting process is more favorable. Moreover, CO need not be the final product, but could react further to yield base chemicals, such as formaldehyde or methanol upon addition of a hydrogen source, just as well as the additional oxygen atom on the surface can take part in various oxidation processes. This kind of more detailed pathway studies will be investigated in a future study.

While we have primarily discussed the thermodynamic effects of the excess electron, the kinetics of the catalytic reaction are also of great importance. As a first assessment of the impact of the surface charge on reaction barriers, estimated transition states of the direct splitting reaction were determined. We find that the presence of a negative surface charge

consistently lowers the energy of configurations with partially broken bonds such as transition states, lowering the estimated splitting barrier on all metals: from 1.15 eV to 0.75 eV on Ti, from 0.80 eV to 0.65 eV on Ni, and from 1.26 eV to 0.83 eV on Cu. Through the presence of an additional electron, partially unsaturated atoms in the transition state receive some additional stabilization, hence lowering the apparent reaction barrier and increasing the reaction rate. It must be mentioned that the calculated barriers do not necessarily reflect the lowest energy splitting pathway, but are chosen so as to provide a consistent set of benchmark configurations. For example, in our CVHD simulations we find that CO_2 splitting on Ti occurs from a rearranged state in which the molecule is bound exclusively on the metal, as opposed to the metal-support bridge we used as initial state here, as shown in Figure 5.

CONCLUSIONS

In the most general sense, electron deposition leads to a chemical reduction of the catalytic surface and, hence, increases its reductive capabilities. Specifically, this phenomenon has a very favorable effect on CO_2 activation, with respect to both adsorption strength and overall reaction energy of the splitting reaction. For the strongly oxidizable adsorbed Ti catalyst, this effect is not as pronounced as for Ni and Cu: while all metals formally adsorb in their M^{2+} state, Ti can easily be further oxidized to Ti^{4+}, allowing it to act as a strong reducing agent without having to be charged, as evidenced by its strong CO_2 activation abilities. The properties of the latter are also largely in line with the redox properties of TiO_2 surfaces, resulting from oxygen vacancy creation and annihilation and which allow for efficient reduction of CO_2.[16,17]

A less general interpretation of the phenomenon involves viewing the negatively charged catalyst as more Lewis basic, which is appropriate for the description of the bare Al_2O_3 support, but is more difficult to apply once adsorbed transition metal clusters have to be

considered, as evidenced by the different behavior of CO adsorbed on the support or the metal, respectively. An analysis of the electronic structure of the adsorption complex hence provides the most valuable and robust insight into its response to surface charging.

The major impact of surface charging on the catalytic performance of supported Ni and Cu—even inducing a reversal of their relative activity—demonstrates that conclusions drawn for "conventional" thermal catalysis not necessarily hold for processes involving charged catalysts in, e.g., a plasma. Indeed, the presence of a large surface charge might help explain often-observed but poorly understood synergistic effects in plasma catalysis.

It remains to be seen to what extent the large excess electron-induced effects observed for the systems and reactions of this study are applicable to other catalysts and processes. Different support materials (e.g., semiconductors rather than isolators), larger supported clusters, transition metal surfaces and a more exhaustive set of redox processes should all be considered in order to assess the influence of a negative surface charge on catalysts in a more general sense. The methodology outlined in this work can provide the template for such a systematic undertaking. However, the results presented in this work already point to a phenomenon with potentially far-reaching consequences: by varying the discharge parameters of the plasma and the degree of electron deposition on the plasma-facing catalyst, its Lewis acidity and redox properties can be modified as well. Thus, controlling the electron deposition on a catalyst opens another avenue towards activity and selectivity control of a plasma-catalytic process.

ACKNOWLEDGEMENTS

K.M.B. is funded as PhD fellow (aspirant) of the FWO-Flanders (Fund for Scientific Research-Flanders), Grant 11V8915N. The computational resources and services used in this

work were provided by the VSC (Flemish Supercomputer Center), funded by the Research Foundation - Flanders (FWO) and the Flemish Government – department EWI

APPENDIX: METHODOLOGICAL DETAILS OF CHARGED SURFACE MODELING

Besides the already mentioned deficiencies of calculations employing simulations cells with a net charge, these approaches also exhibit poor convergence behavior. To assess the influence of the handling of charged slabs on computed properties, we first checked the "straightforward" approach of a slab in a fully periodic cell with a net charge. In Figure 8a, the effect of the cell size (by varying its *Z* length) on both the total energy of a dry slab, as the adsorption energy of CO_2 on it, is shown. Even for very large cells, no clear convergence is observed.

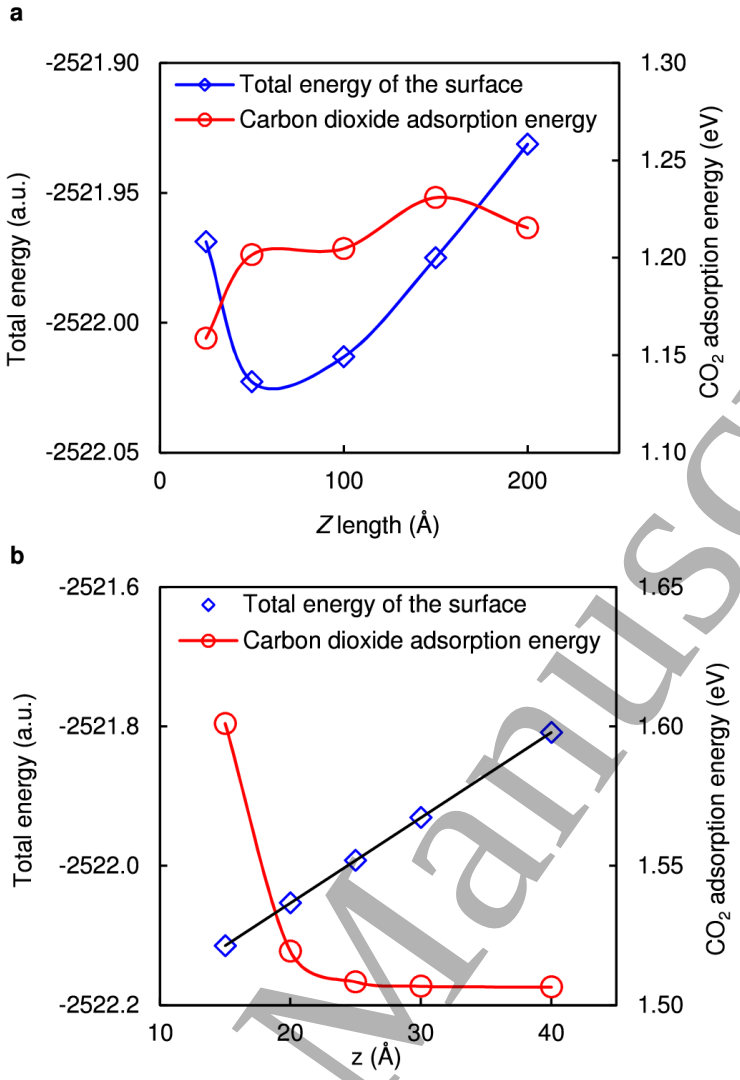

Figure 8: Convergence of computed CO_2 adsorption energies (in the d-IVb configuration) on a negatively charged slab. (a) Negatively charged slab without neutralizing charge and its dependence of the cell size. (b) Negatively charged slab with neutralizing charge and its dependence on the position of the neutralizing countercharge. For the total energies, a straight line is fitted.

The accuracy of the countercharge approach hinges on the assumption that if the energetic contribution from the point charge (besides generating a perpendicular electric field) is the same for all systems, adsorption energies are not affected because its effect is cancelled when subtracting the energies of the slab + adsorbate and the clean slab. To verify this assumption, energies were computed for different Z positions of the countercharge, depicted in Figure 8b, employing a non-periodic *Z* box length of 100 Å.

The interaction energy of the countercharge and the slab is linearly dependent on their mutual distance, which is the expected behavior for two interacting infinite charged plates. At sufficient separation, the effect of adsorbed species on this interaction becomes negligible, and the computed adsorption energy converges. That is, the electrostatic interactions between de surface and the countercharge reduce to a simple plate-plate interaction (with corresponding electric field) in an averaged sense, rather than a point charge-adsorbed molecule interaction that can be observed if the point charge is too close. A *Z*-position higher than 30 Å (or a distance of ~20 Å) suffices, and the value of 40 Å used in our production calculations is a very conservative choice.

REFERENCES

[1] Neyts E C, Ostrikov K K, Sunkara M K and Bogaerts A 2015 *Chem. Rev.* **115** 13408–13446

[2] Zhang A J, Zhu A M, Guo J, Xu Y and Shi C 2010 *Chem. Eng. J.* **156** 601–606

[3] Tu X and Whitehead J 2012 *Appl. Catal. B: Environ.* **125** 439–448

[4] Mei D, Zhu X, Wu C, Ashford B, Williams P T and Tu X 2016 *Appl. Catal. B: Environ.* **182** 525–532

[5] Chen G, Georgieva V, Godfroid T, Snyders R and Delplancke-Ogletree M P 2016 *Appl. Catal. B: Environ.* **190** 115–124

[6] Cheng D, Negreiros F R, Aprà E and Fortunelli A 2013 *ChemSusChem* **6** 944–965

[7] Zhu Y A, Chen D, Zhou X G and Yuan W K 2009 *Catal. Today* **148** 260–267

[8] Grabow L C and Mavrikakis M 2011 *ACS Catal.* **1** 365–384

[9] Yang Y, White M G and Liu P 2012 *J. Phys. Chem. C* **116** 248–256

[10] Liu C, Cundari T R and Wilson A K 2012 *J. Phys. Chem. C* **116** 5681–5688

[11] Wang Z, Cao X M, Zhu J and Hu P 2014 *J. Catal.* **311** 469–480

[12] Dietz L, Piccinin S and Maestri M 2015 *J. Phys. Chem. C* **119** 4959–4966

[13] Ko J, Kim B K and Han J W 2016 *J. Phys. Chem. C* **120** 3438–3447

[14] Foppa L, Silaghi M C, Larmier K and Comas-Vives A 2016 *J. Catal.* **343** 196–207

[15] Pan Y X, Liu C J and Ge Q 2008 *Langmuir* **24** 12410–12419

[16] Sorescu D C, Al-Saidi W A and Jordan K D 2011 *J. Chem. Phys.* **135** 124701

[17] Huygh S, Bogaerts A and Neyts E C 2016 *J. Phys. Chem. C* **120** 21659–21669

[18] Cornu D, Guesmi H, Krafft J M and Lauron-Pernot H 2012 *J. Phys. Chem. C* **116** 6645–6654

[19] Ye J, Liu C and Ge Q 2012 *J. Phys. Chem. C* **116** 7817–7825

[20] Hahn K R, Iannuzzi M, Seitsonen A P and Hutter J 2013 *J. Phys. Chem. C* **117** 1701–1711

[21] Mayi O I, Thiyam P, Bostrom M and Persson C 2015 *Phys. Chem. Chem. Phys.* **17** 20125–20133

[22] Moon H S, Kwon S, Kwon S H, Cho M, Seo J G and Lee S G 2016 *RSC Adv.* **6** 28607–28611

[23] Mishra A K, Roldan A and de Leeuw N H 2016 *J. Phys. Chem. C* **120** 2198–2214

[24] Pan Y X, Liu C J, Wiltowski T S and Ge Q 2009 *Catal. Today* **147** 68–76

[25] Silaghi M C, Comas-Vives A and Copéret C 2016 *ACS Catal.* **6** 4501–4505

[26] Zhang R, Wang B, Liu H and Ling L 2011 *J. Phys. Chem. C* **115** 19811–19818

[27] Ye J, Liu C J, Mei D and Ge Q 2014 *J. Catal.* **317** 44–53

[28] Rodriguez J A, Liu P, Stacchiola D J, Senanayake S D, White M G and Chen J G 2015 *ACS Catal.* **5** 6696–6706

[29] Neyts E C and Bogaerts A 2014 *J. Phys. D: Appl. Phys.* **47** 224010

[30] Huygh S and Neyts E C 2015 *J. Phys. Chem. C* **119** 4908–4921

[31] Somers W, Bogaerts A, van Duin A C T and Neyts E C 2012 *J. Phys. Chem. C* **116** 20958–20965

[32] Shirazi M, Neyts E C and Bogaerts A 2017 *Appl. Catal. B: Environ.* **205** 605–614

[33] Shirazi M, Bogaerts A and Neyts E C 2017 *Phys. Chem. Chem. Phys.* **19** 19150–19158

[34] Heinisch R L, Bronold F X and Fehske H 2012 *Phys. Rev. B* **85** 075323

[35] Ambrico P F, Ambrico M, Schiavulli L, Ligonzo T and Augelli V 2009 *Appl. Phys. Lett.* **94** 051501

[36] Ambrico P F, Ambrico M, Colaianni A, Schiavulli L, Dilecce G and De Benedictis S 2010 *J. Phys. D: Appl. Phys.* **43** 325201

[37] Peeters F J J, Rumphorst R F and van de Sanden M C M 2016 *Plasma Sources Sci. Technol.* **25** 03LT03

[38] Tschiersch R, Nemschokmichal S, Bogaczyk M and Meichsner J 2017 *J. Phys. D: Appl. Phys.* **50** 105207

[39] Kim J, Abbott M S, Go D B and Hicks J C 2016 *ACS Energy Lett.* **1** 94

[40] Rossmeisl J, Skúlason E, Björketun M E, Tripkovic V and Nørskov J K 2008 *Chem. Phys. Lett.* **466**, 68–71

[41] Skúlason E, Tripkovic V, Björketun M E, Gudmundsdóttir S, Karlberg G, Rossmeisl J, Bligaard T, Jónsson H and Nørskov J K 2010 *J. Phys. Chem. C* **114** 18182–18197

[42] Deskins N A, Rousseau R and Dupuis M 2010 *J. Phys. Chem. C* **114** 5891–5897

[43] Yin W J, Wen B, Bandaru S, Krack M, Lau M and Liu L M 2016 *Sci. Rep.* **6**, 23298

[44] Yang X F, Wang A, Qiao B, Li J, Liu J and Zhang T 2013 *Acc. Chem. Res.* **46** 1740–1748.

[45] Liu J 2017 *ACS Catal.* **7** 34–59

[46] VandeVondele J, Krack M, Mohamed F, Parrinello M, Chassaing T and Hutter J 2005 *Comput. Phys. Commun.* **167** 103–128

[47] Hutter J, Iannuzzi M, Schiffmann F and VandeVondele J 2014 *WIREs Comput. Mol. Sci.* **4** 15–25

[48] Lippert G, Hutter J and Parrinello M 1997 *Mol. Phys.* **92** 477–488

[49] Goedecker S, Teter M and Hutter J 1996 J *Phys. Rev. B* **54** 1703–1710

[50] Krack M 2005 *Theor. Chem. Acc.* **114** 145–152

[51] VandeVondele J and Hutter J 2007 *J. Chem. Phys.* **127** 114105

[52] Perdew J P, Burke K and Ernzerhof M 1996 *Phys. Rev. Lett.* **77** 3865–3868

[53] Grimme S, Antony J, Ehrlich S and Krieg H 2010 *J. Chem. Phys.* **132** 154104

[54] Grimme S, Ehrlich S and Goerigk L 2011 *J. Comput. Chem.* **32** 1456–1465

[55] Bultinck P, Van Alsenoy C, Ayers P W and Carbó-Dorca R 2007 *J. Chem. Phys.* **126** 144111

[56] Henkelman G, Uberuaga B P and Jónsson H 2000 *J. Chem. Phys.* **113** 9901–9904

[57] Digne M, Sautet P, Raybaud P, Euzen P and Toulhoat H 2004 *J. Catal.* **226**, 54–68

[58] Martyna G J and Tuckerman M E 1999 *J. Chem. Phys.* **110**, 2810–2821

[59] Wischert R, Laurent P, Copéret C, Delbecq F and Sautet P 2012 *J. Am. Chem. Soc.* **134** 14430–14449

[60] Zhang Y and Yang W 1998 *Phys. Rev. Lett.* **80** 890–890

[61] Tao J, Perdew J P, Staroverov V N and Scuseria G E 2003 *Phys. Rev. Lett.* **91** 146401

[62] Vydrov O A and Van Voorhis T 2010 *J. Chem. Phys.* **133** 244103

[63] Sabatini R, Gorni T and de Gironcoli S 2013 *Phys. Rev. B* **87** 041108

[64] Hujo W and Grimme S 2011 *J. Chem. Theory Comput.* **7** 3866–3871

[65] Patkowski K, Murdachaew G, Fou C M and Szalewicz K 2005 *Mol. Phys.* **103** 2031–2045.

[66] Tribello G A, Bonomi M, Branduardi D, Camilloni C and Bussi G 2014 *Comput. Phys. Commun.* **185** 604–613

[67] Laio A and Parrinello M 2002 *Proc. Natl. Acad. Sci. U. S. A.* **99** 12562–12566

[68] Bal K M and Neyts E C 2015 *J. Chem. Theory. Comput.* **11** 4545–4554

[69] Bal K M and Neyts E C 2016 *Chem. Sci.* **7** 5280–5286

[70] Hub J S, de Groot B L, Grubmüller H and Groenhof G 2014 *J. Chem. Theory Comput.* **10** 381–390

[71] Bal K M and Neyts E C 2017 *Phys. Chem. Chem. Phys*., submitted

[72] Hackett S F, Brydson R M, Gass M H, Harvey I, Newman A D, Wilson K and Lee A F 2007 *Angew. Chem., Int. Ed.* **46**, 8593−8596

[73] Ghosh T K and Nair N N 2013 *ChemCatChem* **5** 1811−1821

[74] Peterson E J, DeLaRiva A T, Lin S, Johnson R S, Guo H, Miller J T, Kwak J H, Peden C H F, Kiefer B, Allard L F,Ribeiro F H and Datye A K 2014 *Nat. Commun.* **5** 4885